CHIN. PHYS. LETT. Vol. 35, No. 12 (2018) 120701

Endoscopic Optical Doppler Tomography Based on Two-Axis Scanning MEMS Mirror *

Dong-Lin Wang(王东琳)[1**], Yun-Qi Hao(郝蕴琦)[1], Feng-Xiao Zhai(翟凤潇)[1], Kun Yang(杨坤)[1], Hong-Qiong Liu(刘洪琼)[2], Qiao Chen(陈巧)[2], Huikai Xie(谢会开)[3]

[1]*School of Physics and Electronic Engineering, Zhengzhou University of Light Industry, Zhengzhou 450000*
[2]*WiO Technology Ltd., Co., Wuxi 214000*
[3]*Department of Electrical and Computer Engineering, University of Florida, Gainesville FL 32611, USA*

(Received 4 June 2018)

We study the feasibility of endoscopic optical Doppler tomography with a micro-electro-mechanical system (MEMS) mirror based probe. The additional phase shifts introduced by the probe are tracked and formulated. The suppression method of the probe phase shifts is proposed and validated by fluid flow detection experiments. In vivo blood flow detection is also implemented on a hairless mouse. The velocities of the blood flow in two directions are obtained to be −8.1 mm/s and 6.6 mm/s, respectively.

PACS: 07.10.Cm, 07.60.−j, 02.60.Gf, 42.30.Rx DOI: 10.1088/0256-307X/35/12/120701

Optical Doppler tomography (ODT) is an important functional extension of optical coherence tomography (OCT), which enables us to measure three-dimensional (3D) distribution of flow velocity in a sample.[1,2] In the last few decades, Doppler imaging algorithms have been proposed by several groups. For example, Zhao *et al.* developed a phase-resolved method and successfully obtained high spatial resolution and high velocity sensitivity at the same time.[3] Barton *et al.* used intensity of OCT images to extract flow information[4] and successfully avoided the unstable phase problem. Others have calculated the phase or intensity variance between adjacent A-scans or B scans in OCT images to conquer the phase unstability problem. Due to its high resolution and velocity sensitivity, ODT enables us to measure flow velocity in blood vessels and even in microvasculatures.[5−7] However, only a few reports on endoscopic ODT have been published because of the stringent size requirement for the probes to access internal organs.

Micro-electro-mechanical system (MEMS) technology has great potential to solve this problem because it has the advantages of creating devices of small size, fast speed and at low cost. A single MEMS mirror can perform two-dimensional (2D) raster scan, and MEMS based endoscopic OCT has been studied by several groups.[8,9] Nevertheless, very few reports on MEMS based ODT endoscopes have been found in the literature. The main reason is that a MEMS probe usually introduces additional phase shift noise into ODT images when the incident light beam is not aligned precisely with the center of the MEMS mirror or the pivot of the MEMS mirror drifts during the MEMS mirror scans. This extra phase shift noise will blur the background phase shift, which limits the velocity resolution. In this work, a modified phase-resolved ODT algorithm is developed to deal with the background phase shift introduced by MEMS based probes.

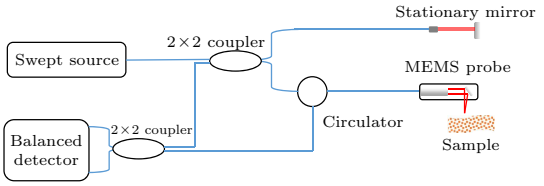

Fig. 1. Schematic of the MEMS based endoscopic swept source optical coherence tomography.

A swept source optical coherence tomography system was developed to study the phase shift of the MEMS probe, as shown in Fig. 1. The laser sweeps in k-space at 50 kHz and generates a linear K-clock sequence for axial scan (A-scan). Its central wavelength is 1310 nm and the bandwidth is about 80 nm. The maximum number of K-clocks in each sweeping period is 1286. In our experiment, we selected 1216 K-clocks for each A-scan, which were converted to 608 depth points. A wavelength-varying narrow-band light generated by the swept source is split via a 2×2 fiber coupler into the reference arm and the MEMS mirror based endoscopic probe. The backscattered light from a sample interferes with the reference light reflected by the stationary mirror at another 2×2 fiber coupler. A balanced photodiode converts two differential light fringes coming out from the coupler into electrical signals and subtracts them to output a voltage signal. After a series of sample signals are recorded on a computer, OCT images can be readily reconstructed through routine OCT data processes including digital filtering, numerical dispersion compensation and fast Fourier transform. The probe can perform fast-axis scans at 50 Hz, which enables real time display

*Supported by the National Natural Science Foundation of China under Grant No 61705199, the Natural Science Foundation of Henan Province under Grant No 162300410317, the Henan Science and Technology Project under Grant Nos 162102310576 and 172102210542, the Zhengzhou Science and Technology Project under Grant No 153PKJGG125, and the US National Science Foundation under Grant No 1002209.

**Corresponding author. Email: kikey7758@163.com

© 2018 Chinese Physical Society and IOP Publishing Ltd

of OCT images on a screen at nearly 50 frame/s, and each frame of the OCT image contains 512 A-scans.

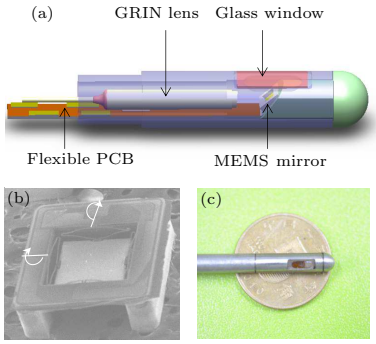

Fig. 2. MEMS mirror based endoscopic probe: (a) 3D model of the probe, (b) dual S-shape bimorph MEMS mirror, and (c) picture of the endoscopic probe.

Figure 2(a) presents the 3D design model of the MEMS probe. It is composed of a mount base, a gradient reflective index (GRIN) lens module, and an MEMS mirror. The MEMS mirror (WiO WM-U2), as shown in Fig. 2(b) has a 0.8 mm×0.8 mm active mirror plate coated with aluminum. It is based on electrothermal actuation and has a unique dual S-shape bimorph structure that can simultaneously achieve 2-axis large scan range at low drive voltage.[10] The MEMS mirror is flip chip bonded on a flexible printed circuit board (FPCB) which provides electrical connection and mechanical support to the MEMS mirror. The GRIN lens module, which is assembled with a single-mode fiber in a glass sleeve, focuses the light into a 15 µm spot at 6.5 mm distance which leads to a 2–3 mm working distance outside of the probe. The GRIN lens has both ends cut with 8° to eliminate artifacts in OCT images caused by the back reflection on the surfaces of the GRIN lens. A mount base made of stainless steel for biocompatibility provides housing and robustness for the probe. Figure 2(c) is a picture of the probe, the outer diameter of the probe is 3.5 mm, and the probe design is similar to the one reported in Ref. [11]. To perform a linear raster scan pattern, the endoscopic probe is driven by triangular waveforms varying from 0 to 3 V to scan at both x-axis and y-axis. The maximum optical scan angle of the probe is about ±12° in both axes. The actuators in x-axis are driven at 50 Hz as the fast scan, while the actuators in y-axis are driven at 0.45 Hz as the slow scan. In this way, 3D OCT images of the sample can be obtained.

Phase-resolved algorithm is popular in ODT to extract flow velocities, which adds a phase shift extraction step to the common OCT image processing.[12] In this work, the flow velocity extraction method is based on the phase-resolved algorithm, and the uniqueness of this work is that it deals with the phase shift generated by the MEMS mirror.

After fast Fourier transform (FFT) of each A-scan interference signal, complex depth data can be obtained. The amplitude of the complex data is used to retrieve OCT structural image, and the phase information is used to extract the Doppler velocity. When a light is incident at an angle of θ on moving particles in a highly scattering medium, a Doppler frequency shift could be observed. The relationship between the particle velocity V and Doppler shift f_{Doppler} can be expressed as

$$V = \frac{\lambda_0 f_{\text{Doppler}}}{2n\cos(\theta)}, \tag{1}$$

where λ_0 is the wavelength of the incident light, and n is the refractive index of the scattering medium. The Doppler frequency shift can be calculated by the phase change, $\Delta\phi$, between two adjacent A-scans; i.e.,

$$f_{\text{Doppler}} = \frac{\Delta\phi}{2\pi T}, \tag{2}$$

where T is the interval between two sequential A-scans, e.g., 20 µs in this work. The phase change of each point can be calculated by the Kasai autocorrelation algorithm,[13] which is given by

$$\Delta\phi_{(i,j)} = \arctan\frac{\text{Im}[\sum_j^{j+N-1} P(\tilde{i},j)\cdot\tilde{P}^*_{(i,j+1)}]}{\text{Re}[\sum_j^{j+N-1} P(\tilde{i},j)\cdot\tilde{P}^*_{(i,j+1)}]}, \tag{3}$$

where the subscripts i and j are the image rows and columns, respectively, N is the number of A-scans used for averaging; e.g., 10 for this work, and $\widetilde{P}_{(i,j)}$ and $\widetilde{P_{(i,j)}}^*$ are the complex signals and their conjugates. After substituting Eqs. (2) and (3) into Eq. (1), we have

$$V_{(i,j)} = \frac{\lambda_0}{4\pi nT\cos(\theta)}\cdot\Delta\phi_{(i,j)}. \tag{4}$$

Finally, the distributed velocities in the medium can be calculated. This phase sensitive method works well in a phase stable system. The maximum measurable velocity may be limited by Eq. (3), because it will wrap the phase in $[-\pi,\pi]$ when the phase change caused is over π radians.

To overcome the four-quadrant arctangent limitation, a phase unwrapping algorithm is required. Two main types of phase unwrapping algorithms are commonly used: path-following method and minimum-norm method. Robust algorithms are time consuming. For simplicity, in this work, the one-dimensional path-following method is adapted to implement phase unwrapping, i.e.,

$$\Delta\phi'_j = \Delta\phi_j - \pi\cdot\text{round}\left[\frac{\Delta\phi_j - \Delta\phi'_{j-1}}{\pi}\right], \tag{5}$$

where $\Delta\phi_j$ is the jth A-line phase shift obtained from Eq. (3) by considering only one dimension, and $\Delta\phi'_j$ is the unwrapped phase shift. The phase shift can be accurately recovered if there are no discontinuous phase changes, but noises and under-sampled conditions may have catastrophic effects on the phase unwrapping process. Nevertheless, this simple method is sufficient and works well for the feasibility study.

In most cases especially in the Fourier domain OCT, scanning devices and other components of the OCT system will generate additional phase shifts.

These phase shifts pose as background phase noises that blur the ODT images and lead to false velocity information. Without background phase noises elimination, velocities will be observed in the ODT images of even a stationary sample. Likewise, small velocity information may be submerged. The background phase noises of the MEMS probe based ODT system includes two parts: one comes from the OCT system, and the other is introduced by the MEMS mirror.

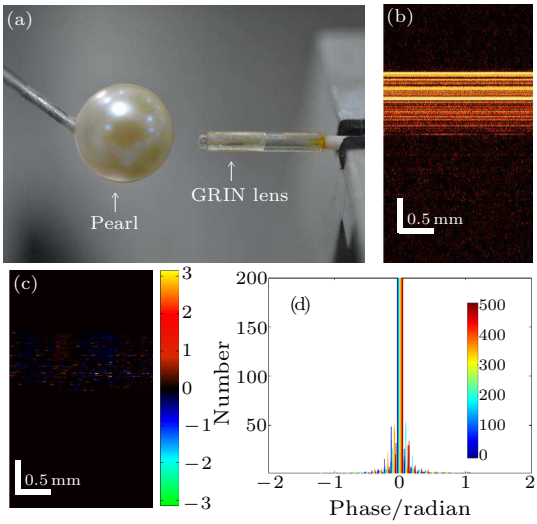

Fig. 3. (a) Using a GRIN lens to image a stable pearl to test the phase noise of OCT system. (b) OCT image of the pearl, white bars represent 0.5 mm. (c) Doppler phase shifts image of the pearl, white bars represent 0.5 mm and color bar represents phase shift value. (d) Histogram bins of the Doppler phase shifts image, and color bar represents different columns of phase shift image.

To present the phase noise of the OCT system without the MEMS mirror, a GRIN lens, the same as the one assembled in the MEMS probe, was fixed to directly image a stationary pearl as shown in Fig. 3(a). Without MEMS mirror scan, the OCT image of the pearl contains only straight lines along B-scan, and Fig. 3(b) shows the same result. However, in the corresponding Doppler phase shift image, significant phase shifts in the sample area are observed in Fig. 3(c), which originate from the OCT system. These phase noises come from the photodetector, light source and interferometer. The phase noise of photodetector mainly includes shot noise and thermal noise, but they are white noises and randomly distribute. In this study they are negligible in ODT images, e.g., in Fig. 3(c), no obvious phase noise exists out of the sample area. The phase noise of interferometer due to the fact that fluctuation is also negligible in short time, but the noise from light source due to laser speckle is obvious. In Fig. 3(c) the sample area displays the speckle phase noise. Figure 3(d) shows the histogram of OCT system phase noises, which are randomly distributed and most of the phase noise values are distributed between −0.5 to 0.5 radians.

The other background phase noise comes from the phase shifts introduced by the MEMS mirror when it scans. To demonstrate this phase noise, a stationary IR card was selected to be imaged by the MEMS probe, and Fig. 4(a) presents the Doppler phase shifts image of the stationary IR card. This displays a range of phase shifts corresponding to a maximum velocity of about 5 mm/s according to Eq. (4), which is definitely wrong because the IR card was not moving at all. Figure 4(b) shows that the phase shifts of the probe are distributed between −0.8 to 1.5 radians, and the phase shifts pattern is a kind of sinusoidal with peaks ramping up.

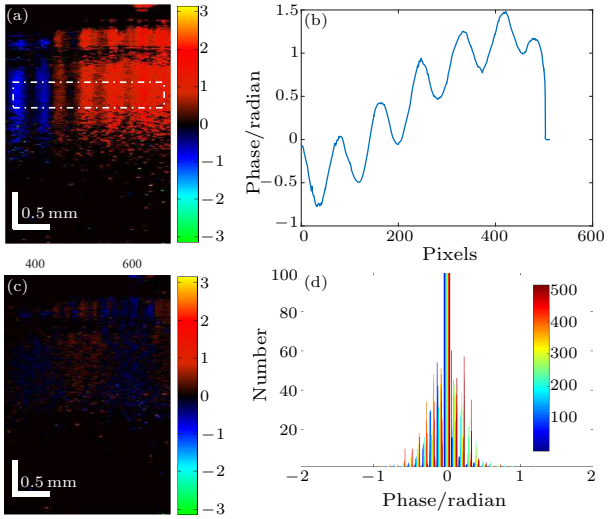

Fig. 4. (a) Doppler phase shifts of an IR card by the probe, white bars represent 0.5 mm and color bar represents phase shift value. (b) Phase shifts introduced by the MEMS probe. (c) Image with probe phase shift subtraction, in which white bars represent 0.5 mm and color bar represents phase shift value. (d) Histograms bins of Doppler phase shifts image, and color bar represents different columns of phase shifts image.

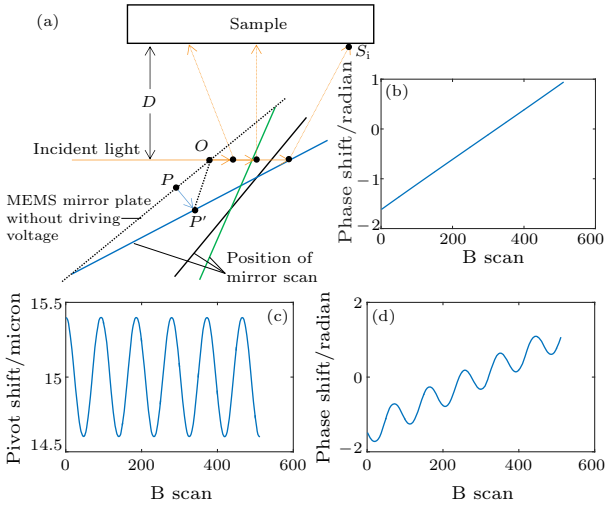

Fig. 5. (a) Illustration of MEMS mirror fast scanning. (b) Phase shifts introduced by MEMS mirror with a fixed rotational center. (c) Pivot shift pattern. (d) Phase shifts in the case of pivot vibration.

To identify the probe phase shifts, let us look into the probe design and fabrication. In practice, it is difficult to produce a perfect MEMS mirror which has no pivot drifting when it scans or to assemble an MEMS mirror based endoscopic probe without any alignment errors. Thus, the optical length of the light incidents

on the MEMS mirror varies as it scans and thus introduces additional phase shifts into Doppler images. To simplify the phenomenon, a one-dimensional transverse scan is executed instead of 2D scan, which means that only one pair of actuators are applied with driving voltages. As shown in Fig. 5(a), the long black dashed line represents the initial position of the MEMS mirror plate without driving voltages and P is the rotation center. Assuming an off-axis incident light propagates on the mirror at point O due to alignment errors, the phase values caused by the optical path of OS at different rotational angles can be expressed as

$$\phi(OS_i) = \frac{2\pi}{\lambda}\Big(\frac{\sqrt{{PP'_i}^2 + OP^2}\sin(\arctan(\frac{PP'_i}{OP}) + \theta_i)}{\sin(45-\theta_i)} + \frac{D}{\cos(2\theta_i)}\Big), \tag{6}$$

where the subscript i stands for the ith transverse scan point, θ_i is the corresponding rotational angle, D is the distance between the sample and incident light, OP stands for the off-axis distance on the mirror, and PP'_i is the MEMS mirror pivot displacement. Subtracting the neighboring phase, the phase shifts introduced by the MEMS mirror can be calculated by

$$\Delta\phi_i = \phi(OS_{i+1}) - \phi(OS_i). \tag{7}$$

Figure 5(b) presents the simulation result of the phase shifts introduced by the MEMS mirror in the case of having a fixed rotation center, while PP' is set to 15 µm according to the recorded maximum value at scan angles between ±3°, OP is 100 µm, and the distance D is 3 mm for the simulation. The result shows that phase shifts are approximately linear with transverse scan points. However, in most cases, the rotational center is not stable but fluctuates during the mirror scanning. If the pivot vibrates, such as the pattern in Fig. 5(c), then the phase shifts become the pivot sinusoidal vibration pattern adding on the straight line, as given in Fig. 5(d). This phenomenon also suggests an interesting way to improve the MEMS assembly accuracy. If the rotation center shift, PP'_i, is recorded, then the alignment error of the MEMS assembly, OP, can be directly monitored via the ODT phase shifts image. In this simulation, the light is horizontally incident on the mirror. For an arbitrary incident light, the reflection and rotation matrices should be applied to determine the inclination. Since the phase shift pattern in Fig. 5(d) agrees with the actual phase shifts in Fig. 4(b), Eq. (6) could be used to determine the alignment error of the MEMS probe by pre-image of a stationary sample and to tract the phase shift values.

To suppress the phase noise introduced by the MEMS probe, a stationary sample could be used to track the phase shift values, and then this phase noise could be suppressed by simple subtraction from the ODT image. In Fig. 4(c) the probe phase shifts are suppressed by subtraction but some residual phase shifts with speckle phase noise left, as shown in Fig. 4(d), present the residual phase noises are distributed between −1 to 1 radians.

The probe phase noise suppression method was validated with a flow phantom. For the purpose of feasibility study, only one pair of the MEMS mirror actuators in the probe was driven to acquire only 2D OCT images. The experiment was carried out on a glass tube filled with flowing milk, which was pumped by a 1 ml graduated syringe. The reflective index of the glass tube is 1.51, and the internal diameter is 1 mm. The milk is a commercial type with a 3% fat volume concentration whose reflective index is about 1.35. The syringe pumped the fluid milk into the glass tube by a linear motor, then the flow velocity of milk in the glass tube could be controlled by the pumping speed. The MEMS probe was fixed at a stage with the optical window facing the glass tube. The light from the probe enters at an angle of 67.5° on the glass tube, and theoretic nominal flow velocity could be calculated by counting the time when the liquid in the syringe was completely pumped into the glass tube.

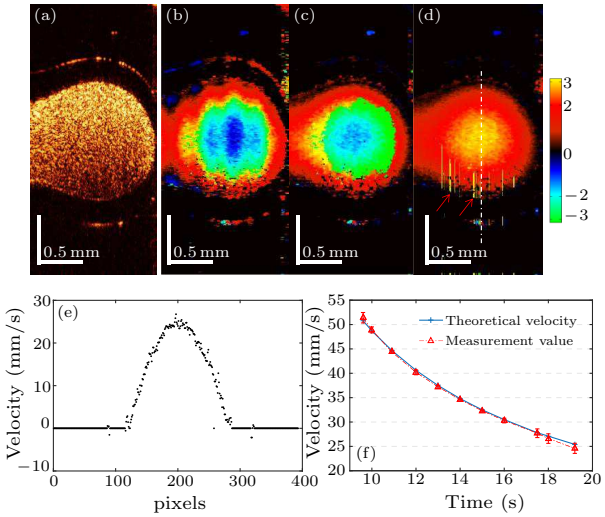

Fig. 6. (a) OCT image of flow phantom. (b) ODT image of flow phantom. (c) Result of probe phase shifts suppression. (d) Image after phase unwrapping. (e) Velocity profile. (f) A series of flow velocity measurement results compared to the theoretic values. White bars represent 0.5 mm, and color bars represent phase value.

Figures 6(a)–6(e) present the sequential images along the process of extracting flow velocity using phase subtraction and phase unwrapping algorithm. Figure 6(a) is an OCT image of the flow phantom and Fig. 6(b) is the phase image obtained by Kasai autocorrelation algorithm. Figure 6(c) is the phase image after subtracted the phase shifts introduced by the MEMS probe, where the circular contours of the tube flow is recovered. In Figs. 6(b) and 6(c), warm color and cold color represent positive and negative flow values, respectively. The milk flowing in the tube is unidirectional, thus the negative flow velocities in Fig. 6(c) are false, and this phenomenon is caused by phase wrapping. The unwrapped phase result is presented in Fig. 6(d), where all the flow velocities are positive. The short lines pointed by red arrows are

caused by the residual phase noises. More robust phase algorithms may be used to solve this problem but real-time display may be scarified. The velocity profile in the center of the glass tube, plotted in Fig. 6(e), agrees with the parabolic distribution of the laminar flow in the tube. Moreover, a series of different flow rates are tested and Fig. 6(f) plots the results compared with the theoretic calculated values. Each flow rate detection was an average of three repeated experiments. The errors of velocity detection are from 0.6 mm/s to −0.7 mm/s, and the maximum standard error is 1.07 mm/s. The well-matched result demonstrates that the ODT system combined with the MEMS based endoscopic probe can realize precise velocity measurement by employing the proposed phase subtraction and phase unwrapping algorithms.

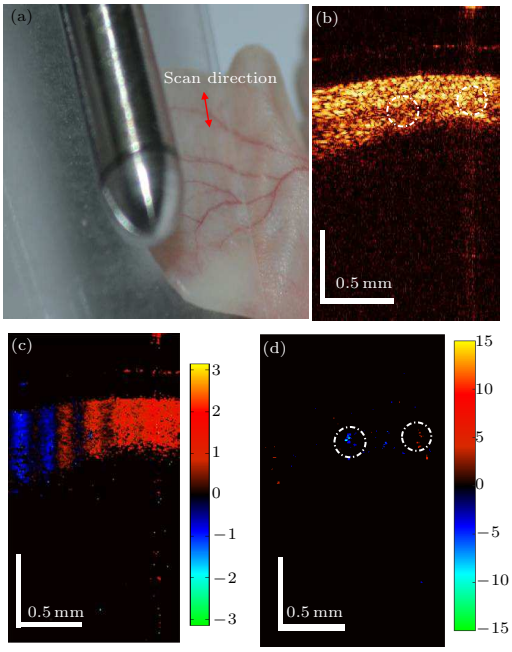

Fig. 7. (a) Scanning blood vessels of a nude mouse ear with the MEMS probe. (b) OCT cross-section image of the mouse ear, and white bars represent 0.5 mm. (c) ODT image of the mouse ear, white bars represent 0.5 mm and color bar represents phase value. (d) Velocity map of the mouse ear with background phase shifts subtraction, white bars represent 0.5 mm and color bar represents velocity value.

An vivo ODT experiment was also performed with the MEMS probe. An anesthetized nude mouse was put on a stage with its ear fixed by a cover glass to eliminate breathing fibrillation, as shown in Fig. 7(a). The probe was guided by a visible light and it scanned visible blood vessels in the mouse ear with an incident angle of 31°. There were flickering pixels in the realtime display of OCT structural images, indicating that flowing blood was present; as shown in Fig. 7(b). Figure 7(c) shows the direct phase Doppler image, in which the phase shifts of flowing blood are overwhelmed by the background signals and the locations of the flowing blood can be hardly identified. By subtracting the phase shifts introduced by the MEMS probe, two blood vessels can be identified. Figure 7(d) shows the blood flowing in the opposite directions, and the velocities of the blood flow in two directions are 8.1 mm/s and 6.6 mm/s, respectively. Note that the velocity detection relies on the incident angle and distance between the MEMS probe and the moving object. Each of the two parameters could be divided into two parts: the first is between the probe and the sample surface (scanning plane), and the second is between the vessel and the scanning plane. In practice, it is recommended to use a robotic arm to keep the probe stable and to control the two vector parameters, and the probe scanning angle at each of A-scan can be obtained.[11] The values between the vessel and scanning plane can be measured by digital image processing technology after ODT 3D reconstruction. An arbitrary slicing function by visualization toolkit (VTK) could be useful for the curved vessels. Overall, there are plenty of engineering methods that can be used to measure the distance and angle values.

In summary, we have presented a feasibility study using an MEMS mirror based probe in a Doppler SS-OCT system. The background phase shifts introduced by the MEMS probe seriously deteriorate the ODT images. These phase shifts can be conveniently obtained by a stationary sample. The experimental results prove that the ODT images can be significantly improved simply by subtracting the MEMS-induced phase shifts. Both phantom and in vivo animal experiments have been performed and the flow velocities of milk in a glass tube and blood vessels in the mouse ear have been successfully measured. Based on these results, the MEMS probe is capable of performing 2D raster scan for ODT images and a 3D ODT reconstruction could also be available in the near future.

References

[1] Huang D, Swanson E A, Lin C P et al 1991 *Science* **254** 1178
[2] Wang X J, Milner T E and Nelson J S 1995 *Opt. Lett.* **20** 1337
[3] Zhao Y, Chen Z, Saxer C et al 2000 *Opt. Lett.* **25** 114
[4] Barton J and Stromski S 2005 *Opt. Express* **13** 5234
[5] Tearney G and Kang D 2017 *Lasers Surgery & Medicine* **49** 249
[6] Haindl R, Trasischker W, Wartak A et al 2016 *Biomed. Opt. Express* **7** 287
[7] Chen C, Cheng K H, Jakubovic R et al 2017 *Opt. Express* **25** 7761
[8] Jung W, McCormick D T, Zhang J et al 2006 *Appl. Phys. Lett.* **88** 163901
[9] Wang D L, Fu L L, Wang X et al 2013 *J. Biomed. Opt.* **18** 086005
[10] Tanguy Q, Bargiel S, Xie H K et al 2017 *Micromachines* **8** 146
[11] Wang D L, Liang P, Samuelson S et al 2013 *Biomed. Opt. Express* **4** 2066
[12] Wang Y, Wang Y M, Guo S G et al 2004 *Opt. Commun.* **242** 345
[13] Yang V X D, Gordon M L, Mok A et al 2002 *Opt. Commun.* **208** 209